We are IntechOpen, the world's leading publisher of Open Access books Built by scientists, for scientists

4,800
Open access books available

122,000
International authors and editors

135M
Downloads

Our authors are among the

154
Countries delivered to

TOP 1%
most cited scientists

12.2%
Contributors from top 500 universities

WEB OF SCIENCE™

Selection of our books indexed in the Book Citation Index in Web of Science™ Core Collection (BKCI)

Interested in publishing with us?
Contact book.department@intechopen.com

Numbers displayed above are based on latest data collected.
For more information visit www.intechopen.com

Chapter 5

Mineralization of Lipid A-Phosphates in Three- and Two-Dimensional Colloidal Dispersions

Henrich H. Paradies, Peter Quitschau, Hendrik Reichelt, Chester A. Faunce and Kurt Zimmermann

Additional information is available at the end of the chapter

http://dx.doi.org/10.5772/48493

1. Introduction

Crystal growth and crystal nucleation has attracted interest for centuries and goes back to Johannes Kepler [1] in 1611. Though progress in the understanding of crystal nucleation and crystal growth were theoretically developed, exact quantitative prediction of the nucleation rates and their kinetics still remains unresolved [2]. As early in 1959, the protocol of preparation of virus crystals and their physical analysis revealed an interparticle spacing of 250 nm [3, 4]. The crystal growth from microcrystalline material to single crystals of viruses marked another event for crystal nucleation. It was concluded for this *Tipula* iridescent virus that the hydrated virus particles in the crystal are not in contact but are separated by large distances of water (~ 50 nm) showing soft modes in the direction of a lattice site and the lattice displacements at a given time is caused by a longitudinal phonon with a wave vector at the zone boundary [5, 6]. These crystals are probably held together by long-range forces operating at a distance comparable with the size of the particles themselves. This is very similar to the recently discovered *autovaccines* obtained from non-pathogenic *E. coli* as liquid colloidal and solid nanocrystals [7-11]. The former virus crystals as well as the discussed liquid *autovaccine* crystals seem to present the well-established instance of a unique ordering of iso-dimensional colloidal particles in three dimensions in solutions and in the solid state. This holds also for the prediction of polymorphic crystal forms like liquid crystals, especially for complex crystalline solid forms originating from colloidal dispersions of e.g. chiral Lipid A-phosphates [12], cationic lipids [13-17], anionic surfactants [18], diblock copolymers [19], or surfactant-water complexes [20]. Crystallization, phase transitions and crystal growth remain a central topic of condensed matter physics. A detailed understanding of the controlled formation of crystalline materials is of great importance for

numerous applications, especially for colloidal particles [21-23], biomimetic approaches to mineralization [24], curved crystalline shapes that emerged from mixtures of barium or strontium carbonates and silica in alkaline media [25], and usually from devices derived from self-assembly of colloidal materials [26, 27].

2. Overview

In view of the above mentioned and widely accepted explanations and morphological descriptions of crystal, nuclei formation and phase transformations, the focus of this contribution relies on recent advances in the physical understanding of the disorder-order, fluid-crystal-fluid transitions of Lipid A-phosphates, the formation of a re-entrant phase, particularly for Lipid A-diphosphate e.g freezing and melting, and the molecular mimicry of hierarchical self-assembly of Lipid A-phosphates. This was achieved using a variety of experimental techniques e.g. scanning electron microscopy (SEM), high resolution transmission electron microscopy (HRTEM) and small-area electron diffraction (SAED), small-angle X-ray diffraction & solution scattering (SAXD & SAXS), static & quasi-elastic light scattering (LS & QELS). The contribution is outlined as follows: In remainder of the brief introduction, a short description is given which is devoted to the chemistry and importance of this class of molecules ("nano-medicine") in the day-to-day life. In Section 3, the phase transition of Lipid A-diphosphate clusters, the formation of various crystal forms as a function of particle number density (n) or volume fraction (ϕ), ionic strength (I) and T will be introduced since they affect the crystallization in 2d and 3d. Observations on freezing and melting of Lipid A-diphosphate clusters on a physical molecular level are also presented. The occurrence of the re-entrant fluid phase of Lipid A-diphosphate clusters upon addition of μM NaOH after a crystalline BCC phase will be compared with the various crystalline phases upon decreasing I and increase of n for NaCl. The self-assembly of Lipid A-diphosphates clusters composed of different "subunits" e.g. six-hexaacylated chains and the corresponding Lipid A-diphosphate with four acylated fatty acid chains with the same phosphorylated disaccharide will be discussed in more detail (crystals, symmetry packing). These crystalline Lipid A-diphosphate cluster complexes may be called "*autovaccines*" (*Note:* An immunizing agent is composed of a selected or modified chemical entity of an original microorganism or virus, which does not cause clinical signs associated with the parent microorganism or virus, but still infects & multiplies in the host so as to induce immunity). Section 4 reports on the formation of Lipid A-diphosphate crystals by surface-induced gradient-induced crystallization in monolayers, their thermodynamics with relation to surface tension and their morphologies. In Section 5 the conclusions are presented.

2.1. Chemistry and the biological role of Lipid A-diphosphate

The lipopolysaccharides (*LPS)* are a group of diverse lipid-containing carbohydrates that exhibit a wide variety of biological activities. They occur naturally on the outer cell membranes of Gram-negative bacteria such as *Escherichia coli.* Although the lipopolysaccharides are large molecules, most of their biological activities result from the

activity of a small portion of the molecule known as Lipid A-diphosphate. The structure of Lipid A consists of two β (1,6)-linked D-glucosamine units with polar phosphate groups at 1 and 4' positions (Fig. 1) [28]. This problem caused approximately 21 000 mortalities in 1996 in the U.S. alone [29].

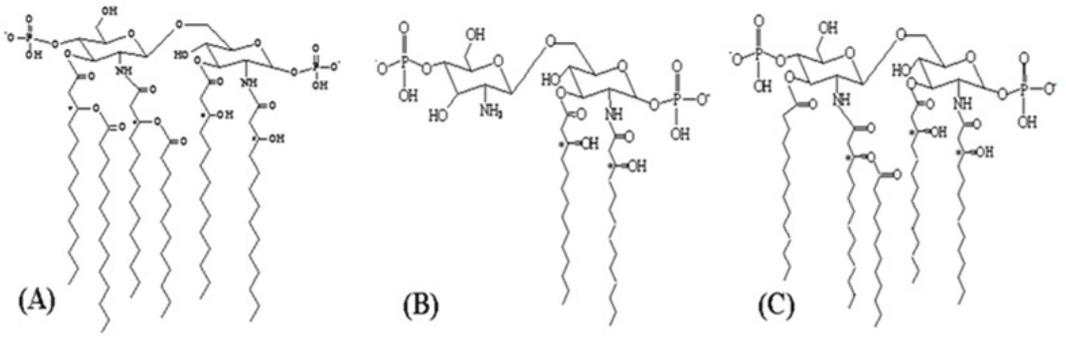

Figure 1. Chemical structures of Lipid A-diphosphate (A) and two Lipid A-diphosphate derivatives (B & C) with strong biological implication on the anti-inflammatory mediator level [28, 30]. Lipid A-diphosphate from *E. coli* is a 1,4-di-phosphorylated β-1,6-linked D-glucosamine disaccharide with four residues of amide-and O-esterified R-(-)-3-hydroxy fatty acids (* denotes the chiral centers in the hydroxy fatty-acid esters), apart from the chiral and epimeric carbons in the glucosamine moieties which are not marked. The antagonistic Lipid A-diphosphate molecules shown in B & C contain the same disaccharide as in (A); however, they differ in the number anchored carbohydrate positions and the number of chiral fatty-acid chains but the chain lengths is the same. The monophosphate of Lipid A is only phosphorylated at the reducing end of the disaccharide (C-1).

The Lipid A-diphosphate is associated with lethal endotoxicity, pyrogenicity and specific immune response. It is also responsible for triggering a cascade of cellular mediators, e.g. tumor necrosis factor α, interleukins, leukotrienes, thromboxane A2 from monocytes and macrophages. The Lipid A-diphosphate and their analogues are distinct from normal lipids with respect to structure, chirality and chemical building units (Fig. 1) [30]. The 2 and 2' amino positions and the 3 and 3' hydroxyl groups are esterified with hydroxy fatty acids. It is known that natural Lipid A-phosphates and approximants are potent immunostimulants which induce a number of desirable effects but also some undesirable ones [30]. Various analogues of Lipid A-diphosphate have been developed to avoid such unwanted effects as toxicity and pyrogenicity, and therefore, they are very distinct from other lipids and surfactants.

Lipid A-diphosphate and approximants possess beneficial effects in clinical therapy against chronic inflammatory diseases and are capable of decreasing resistance to antibiotics and cationic antimicrobial peptides (CAMP) [31]. In this context the CAMP play also a significant role in the immune reaction to gut commensals (inflammatory bowel disease (Crohn), ulcerative colitis) and possibly in antibiotic resistance [30, 31]. This infers to an increased bacterial invasion of the surface of the respective tissues accompanied by the loss of the protective barrier. This accounts for bacterial contamination of the intestinal surface where host and invader are physically in close contact. Accordingly, this view strongly supports the production of "*intestinal autovaccines*" and its therapeutic potential e.g for

protection of CAMP synthesis and sustaining remissions. The chemical structure of the pro-inflammatory component of *LPS*, Lipid A (Fig. 1), varies between bacteria of different species where the Gram-negative bacteria modulate the structure of their *LPS*.

3. Fluid-solid phase transition of self-assembled Lipid A-diphosphate cluster

By applying freeze-fracture electron microscopy and X-ray diffraction techniques a qualitative phase relationship of Lipid A-diphosphate has been reported [32, 33]. These results were taken from samples of Lipid A extracted from Salmonella Minnesota, E. coli rough mutant LPS and from Salmonella enterica serovar Minnesota. In their qualitative study the aqueous specimens have been examined in the presence of mM phosphate buffers by synchrotron radiation and analyzed by their diffraction profiles e.g. cubic, hexagonal or simple cubic structures. However, there ionic strength was a magnitude higher than the one used for preparing electrostatically stabilized Lipid A-diphosphate dispersions with $I = 10^{-4}$ to 10^{-6} M [12]. Especially, SAXD and SAXS are very suitable to characterize the 3-d structure or ordering in solution of the self-assembled Lipid A-phosphate clusters and probe their corresponding long-range order parameters. For comparison with light scattering, the most important advantage of the applied X-rays is their low refractive index contrast (the difference in index of refraction is of the order of 10^{-6}), so the occurrence of multiple scattering and incoherent background scattering is significantly reduced and a much wider range of scattering vectors are available. It was observed that upon reaching a nanocluster size of 500 – 600 nm the suspensions became iridescent to visible light: thus, the iridescence acts as a visual marker of nanocluster size. Recently, the iridescent solutions have been physically analyzed and interpreted in terms of mass, surface charge, size and shape. The influence of polydispersity in charge, size and mass has been elucidated and included in all further experiments and simulations [7-13]. The most compelling observations of the colloidal crystallization and also of Lipid A-diphosphates in aqueous solutions at very low ionic strength conditions ($< 10^{-6}$ M) are the order-disorder transition and the structural transition from a body-centered cubic (BCC) to a face-centered (FCC) structure [34, 35]. In these dispersions it is essential to consider the co-occurrence of phase separation and crystalline ordering, where it has been suggested that the crystalline phase is a supercooled liquid phase with some liquid retained in a metastabile state for a certain period of time, even at $\phi > 0.58$. Experimental phase diagrams of Lipid A-diphosphate dispersions in NaCl or NaOH as shown in Fig. 2 are very helpful in searching for crystal formation, order–disorder as a function of ionic strength I, n and T. Moreover, they are useful for comparison with the theoretical predictions [36, 37]. Normally the crystalline arrays form spontaneously through self-assembly of charged colloidal Lipid A-phosphate spheres in low ionic strength but at low polydispersity in size, mass and charge. The spontaneous formation of self-assembled Lipid A-diphosphate crystallization is mainly driven by the excluded-volume entropy. The decrease in entropy in the colloidal crystals is associated with a nonuniform mean density, however, a greater local volume that each particle can independently explore compensates for these phenomena. If the amount of base (c_s) were increased, a new fluid re-

entrant disordered phase of self-assembled Lipid A-diphosphate clusters was encountered followed by a fluid ordered-crystalline BCC phase for low *n* when using NaOH as an electrolyte in the crystallization process.

3.1. Freezing and melting

It was possible to prepare stable aqueous colloidal dispersions of Lipid A-diphosphate and their approximants with low polydispersity in shape, size, and charge over a discrete range of volume fraction, ϕ [9-11]. The phase transitions were a correlated liquid phase, a cubic FCC and a body-centered cubic crystalline phase [35]. These phases were detected in the presence of mM NaCl for different volume fractions, ϕ; and various crystal forms (BCC and FCC) could be obtained. It was found that these assemblies were consistent with an assembly for a BCC lattice (*Im3m*) with *a* = 35.5 nm. However, a mixture of equimolar concentrations of the two antagonistic molecules revealed a SAXS-powder diffraction pattern a light scattering profile for crystals of sizes of 1 μm that could be indexed for a much larger face-centered (*Fd3m)* unit cell, with *a* = 58.0 nm. However, when employing the similar conditions for colloidal Lipid A-diphosphate dispersions but through addition of μM NaOH rather than by removing NaCl [35] a very different phase behavior was observed (Fig. 2). By varying the amount of added NaOH (or NaCl) it was possible to determine the effective charge, $\overline{Z_{eff}}$ for various *n* values and the screening parameter, *k,* for the excess electrolyte (c_s). For sufficiently large values of *n*, Lipid A-diphosphate crystallized through an increase in $\overline{Z_{eff}}$ at a constant c_s when adding μM NaOH. When the c_s were increased, the crystals melted with little change in $\overline{Z_{eff}}$. An increase in the c_s enhanced interparticle interaction and attraction due to many-body effects (NaOH), but influences long-range interactions where particles repel one another at large separation distances in the presence of NaCl; thus repulsion increases with decreasing particle-particle separation and decreasing ionic strength. The effective charge and $k = 4\pi k_B T \lambda_B (n Z_{eff} + 2 \cdot 10^3/N_A \cdot c_{se})^{1/2}$, with λ_B = 0.735 nm, the Debye screening length, account for counterion condensation and many-body effects. - If the effective charge determined from scattering measurements was used in the simulations, the equilibrium phase boundaries were consistent with predicted universal melting-line simulations [36, 37]. It seems that the presence of NaOH in the aqueous dispersions of Lipid A-diphosphate stabilized a two-state structure. The stabilizing effect was promoted by long-range (counter-ion mediated) attractive interactions between the crystalline clusters and the many-body effects. This Lipid A-diphosphate cluster is able to undergo both a fluid-order and an order-fluid transition.

When the NaOH concentration and the particle-number density of Lipid A-diphosphate is increased, the length scale of the repulsion decreased, because of many-body effects and the disorder-order-transition occurred at a particle-number density close to the freezing transition. When the NaOH concentration and the particle-number density of Lipid A-diphosphate is increased, the length scale of the repulsion decreased, because of many-body effects and the disorder-order-transition occurred at a particle-number density close to the

freezing transition. At lower particle-number densities, as the length scale of the repulsive forces increased, the fluid-crystalline transition gave rise to BCC-type crystals.

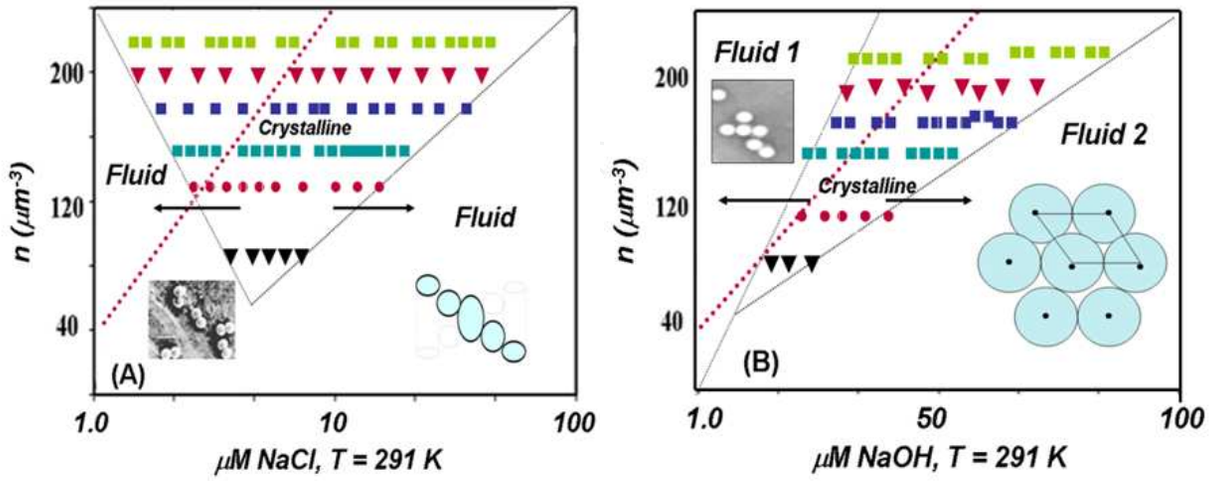

Figure 2. Experimental phase diagrams of self-assembled charged Lipid A-diphosphate and their approximants at constant temperature (T = 291 K) as a function of particle number density, *n*, and ionic strength (*I*). **(A)** Ordered crystal phases appeared after considerable reduction of (*I)* with a large Debye length (NaCl) due to a stabilized electrostatic repulsion between the various self-assembled Lipid A-diphosphate clusters: ▼ Lipid A-diphosphate (A in Fig. 1) crystals; ● self-assembled Lipid A-diphosphate clusters comprising of Lipid A-diphosphate (A) and (C) shown in Fig. 1; ■ self-assembly of Lipid A-diphosphate clusters with (A) and (B) components; ■ self-assembly of components B and C; ▼ self-assembly of component (A) with six chains & with two double chained Lipid A-diphosphate at the non-educing end of the disaccharide; ■ self-assembly of the Lipid A-diphosphate approximant C (Fig. 1). *Inset:* Single spherical Lipid A-diphosphate clusters with d = 70.0 nm (SEM image). They form because of low shape and charge polydispersity (≤ 10%). **(B)** Phase diagram of charged spherical Lipid A-diphosphate clusters with the same composition as in **(A),** however, in the presence of μM NaOH**.** The re-entrant melting lines are shown at the left boundary (charging) and at the right boundary (screening), respectively. The two-phase regions are indicated as horizontal arrows. The red dotted lines indicate the equivalent titration points obtained from conductometric titrations. The·●●●lines are theoretical fits to the experimental data applying an effective charge of $\overline{Z}_{eff} = 345 \pm 76$ for the left boundary, for the right boundary at maximum interaction the effective charge was $\overline{Z}_{eff} = 320 \pm 50$. The corresponding values for NaCl (**A)** were $\overline{Z}_{eff} = 470 \pm 61$ and $\overline{Z}_{eff} = 500 \pm 50$, respectively. **Insets***:* An ordered hexagonal columnar phase of non-crystalline Lipid A-diphosphate in the aqueous dispersion (Fluid 2) in (B) at high μM NaOH, contrary to (A)**.** Lipid A-diphosphate clusters of diameter d = 6.0 nm are only present in the Fluid 1 Phase (SEM image) in (B), whereas the Lipid A-clusters in the hexagonal Fluid Phase 2 exhibit a nearest neighbor distance of 35.1 nm and a packing fraction of 0.68.

This implies that self-screening was much smaller than in previous studies and very different for Lipid A-monophosphate phases [38]. The experimental observations and the simulation support the existence of a transition from a fluid to a BCC structure rather than to an expected FCC structure for Lipid A-diphosphate clusters in e.g 5.0 mM NaCl. However, there was no FCC structure present for a certain NaOH concentration, but there

was a crystalline BCC phase present between two clearly defined fluid phases with no crystals. It was rather unusual to encounter BCC structures for ionic strengths of different magnitude (5.0 μM NaCl vs. 50.0 μM NaOH) and for the same n, therefore, the OH- ions must contribute to the scenario. It is also feasible that the structural transition path was influenced by topological dissimilarities but differently forms the corresponding Lipid A-monophosphate crystalline phase, because of altered elastic deformations between the crystalline BCC phase which formed and the fluid phases from which it originated. The nearest-neighbor interparticle distance, $2d_{exp} = 2\pi/Q_{110} = 32.2$ nm was estimated from the experimental peak positions and compared with the average theoretical distance, $2\ d_{th} = \sqrt{3}/\sqrt[3]{4n}$, for various n, 20 $\mu m^{-3} \leq n \leq 400\ \mu m^{-3}$. For this limited particle-number density range the double-logarithmic plot of $2\ d_{exp}$ and $2\ d_{th}$ vs. n revealed a straight line with a slope of -0.32. The nearest-neighbor distance in the re-entrant fluid phase was determined as $d_{N\text{-}N} = 33.0$ nm, surprisingly for all Lipid A-diphosphate clusters including those with different "subunits". The nearest-neighbor distance for the fluid phase before freezing was found to be $d_{N\text{-}N} = 32.2$ nm. The nearest-neighbor distance for the crystalline phase revealed a value of $d_{N\text{-}N} = 30.8$ nm. This value was expected to be smaller than the average interparticle distance $2d_{th} = 32.2$ nm when a homogeneous particle distribution was assumed with cubic bcc symmetry.

The observed intersphere spacing was normally close to the calculated mean sphere distance except at the interfacial region of the dispersions, where there was contact with the air or a wall. Melting is initiated when the amplitude of vibration becomes sufficiently large for the occurrence of partly shared occupancy between adjacent particles. It occurs when the root mean square of the vibration amplitude of a crystal exceeds a threshold value (~ 0.15 $d_{N\text{-}N}$) according to Lindemann [39] and it would result in a movement of ~ 6.0 nm, which is a distance significantly smaller than the spacing between the surfaces of any of the spherical colloidal Lipid A-diphosphate clusters and a distance much less than the screening length. The Lindemann rule does not hold for crystals in 2d which have quasi-long-range instead of long-range translational order [40]. Measurements of the short-time and the long-time diffusion constants by quasi-elastic light scattering yielded a ratio of ~ 11 in the freezing region for the Lipid A-diphosphate cluster [41]. Furthermore, the possibility exists that the charge deduced from the melting line was also essential to center the particle within the cubic BCC unit cell. *Note*: According to the rule of Verlet and Hansen [42], crystallization occurs when the structure factor of ordinary liquids exceeds a value of 2.85 for 3d and ≅ 4 in 2d. Furthermore, when plotted S(Q) and n on a double-log graph a value of $d_f = 1.75$ was obtained, where S(Q) is the effective structure factor, Q is the scattering vector, d_f is the fractal dimension and close to the one found for a diffusion-limited cluster aggregation of 1.80.

This result may explain why the Lipid A-diphosphate basic arrays adopted the form of colloidal clusters at low particle-number densities and low NaOH concentrations. The number of seeding Lipid A-diphosphate clusters of $\bar{d} = 7$ nm required to form a fractal nucleus of a given size was considerably lower than the number required for a compact

nucleus. These parameters determined whether or not small clusters or sub-critical nuclei developed. Once formed, further cluster growth took place if a sufficient supply of Lipid A-diphosphate clusters of $\bar{d}$ = 7 nm were available. Therefore, cluster growth depended upon n, the size and the charge polydispersity and the availability of residual Lipid A-diphosphate clusters. A further increase in the NaOH concentration resulted in crystal melting and a re-entry into the fluid phase. The morphology of the clusters detected in such dispersions was similar to those of the Lipid A-diphosphate clusters observed before freezing took place. At a sufficiently high concentration of μM NaOH, where strong interactions occurred, freezing can take place and a two-phase region was formed. If the μM NaOH was increased there was an increase in charge on the self-assembled Lipid A-diphosphate clusters according to $R–H_2PO_4H + OH^- \rightarrow R–HPO_4^- + H_2O$. At low μM NaOH, the Lipid A-diphosphate clusters retained their BCC structure. With additional increases in the μM NaOH the interactions became screened with neither an increase nor a decrease in charge and the system began to melt. Although the Lipid A-diphosphate samples investigated covered a limited pH-range ($4.5 \leq pH \leq 7.5$), there was a sufficient excess of NaOH to attribute the re-entrant occurrence to added screening produced by the excess. This is completed different form the situation using NaCl. Because of the Lipid A-diphosphate cluster counterions, the screening parameter, κ increased steadily if $n^{-1/3}$ remained constant. As a result, a decrease in the equilibrium-state lines will be observed and the melting line was crossed. This accounted for the maximum interaction equilibrium state line when the surface charges approached their highest value. Consequently, any further addition of μM NaOH screened the Lipid A-diphosphate particle surface charge and initiated a reduction in the cluster-cluster interaction. The screening parameter, κ, then depended only on the screening electrolyte (NaOH or NaCl). The result was an increase in the equilibrium state lines which again crossed the melting line.

3.2. BCC and FCC structures of Lipid A-phosphates

Some new crystalline Lipid A-diphosphate clusters and their approximants have been developed since the protocol for obtaining electrostatically stabilized solutions of Lipid A-diphosphates or for the corresponding monophosphates at various n was available [11-13]. The well-ordered Lipid A-diphosphate clusters and the presence of higher order diffraction peaks corroborated the existence of crystalline Lipid A-diphosphate material documented for the BCC and FCC structures assigned to the space groups $Im\bar{3}m$ & $Fd\bar{3}m$ [43] depicted in Figs 3 and 4. It was observed that the (211) peak at c_S = 3.15 μM NaOH and the height of this reflection increased with n holding c_B constant (Fig. 3). In addition the sensitivity of Lipid A-diphosphate clusters on pH is illustrated in Fig. 5B. The absence of the specific reflections (Figs. 3B, 4 & 5) of the X-ray diffraction patterns and small-area electron diffraction pattern reinforced the argument that the lattice type was face-centered cubic, therefore, two space groups were possible, namely $Fd\bar{3}$ and $Fd\bar{3}m$.

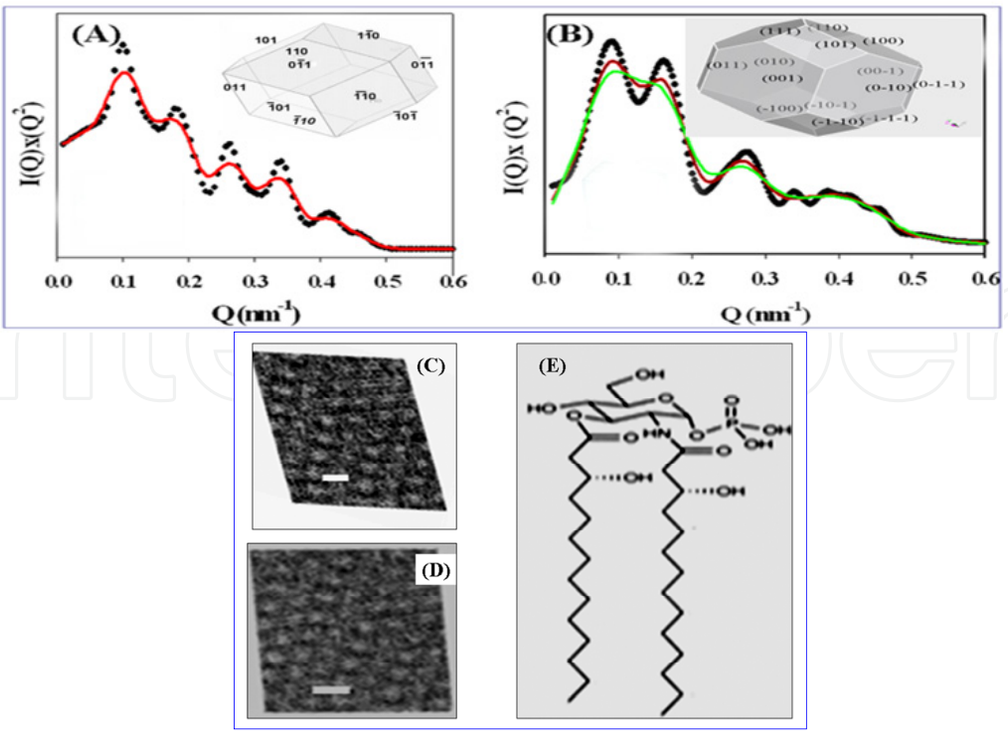

Figure 3. (**A**) SAXS profiles I(Q) vs. Q, with Q = (4π/λ)·sinθ/2), of BCC type colloidal crystals (λ = 1.54 nm) with a = 37.6 nm composed of Lipid A-diphosphate and "subunit" C (Fig. 1) . The assigned space group was *Im3m*, origin at center m3m, and equivalent positions 0, ½, ½; ½, 0, ½; ½, ½, 0 (Q^{229}) based on the molecular composition and the assumed spherical diameter of *d* = 7.0 nm which was consistent with form-factor scattering at higher Q. The black dotted scattering profile is for the Lipid A-diphosphate phase at $\phi = 3.5 \times 10^{-4}$, *I* = 0.5 mM NaCl, the solid-red line is the profile for an equimolar mixture of the antagonistic molecule depicted in B of Figure 1 for Lipid A-diphosphate with *a* = 35.5 nm. (**B**) SAXS profiles of colloidal crystals of the FCC type ($Fd\bar{3}m$), the black-dotted line corresponds to Lipid A-diphosphate with *a* = 57.5 nm comprising of the components A and B (Fig. 1). The red-solid line is for the colloidal mixture of Lipid A-diphosphate and antagonistic Lipid A-diphosphate [47] (Fig. 1B) both are at $\phi = 5.4 \times 10^{-4}$, I = 0.5 mM NaCl. The green solid SAXS profile represents the results from a mixture of Lipid A-diphosphate with the corresponding monosaccharide of Lipid A-diphosphate at $\phi = 3.4 \times 10^{-4}$, I = 0.5 mM NaCl. **Insets:** Crystal morphologies as they appear in SEM images and simulated with the *Accelrys Software Materials Studio 4.4 Module Morphology Version 6.0,* San Diego (USA). The corresponding TEM images are shown in (C) and (D); the scale bar is 10 nm; (D) illustrates the chemical structure of the antagonistic Lipid A-diphosphate [47] composed only of a diphosphorylated glucosamine residue and two fatty-acid chains.

The two space groups were also centrosymmetric and belong to the Laue classes $m\bar{3}$ and $m\bar{3}m$. *Note:* $Fd\bar{3}m$ corresponds to special positions of $Fd\bar{3}$. The observed and calculated *hkl* sets of Bragg reflections were consistent with a combination of different sites in the $Pm\bar{3}n$ (*a* and *d*), or of sites *a* and *d* in the $Fd\bar{3}m$ (Fig. 5). High-resolution transmission electron microscopy, SAED on crystalline Lipid A-diphosphate rods of the order of 2-3 μm in length and diameters of several nm obtained at pH 8.0 [45] revealed that the rods were held to the truncated polyhedra with a five-fold symmetry (Fig. 6).

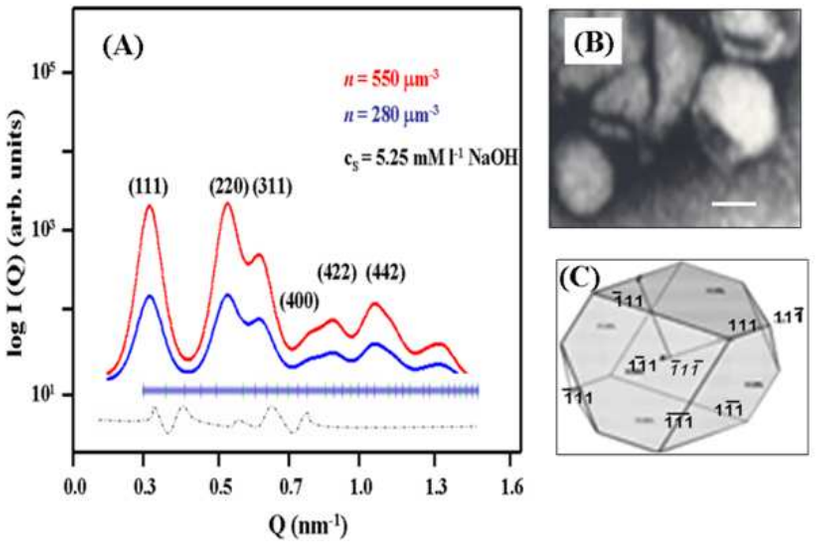

Figure 4. **(A)** S(Q) vs. Q profile for colloidal FCC-type crystals of Lipid A-diphosphate clusters with a = 57.0 nm for n = 140 μm^{-3} and cs = 2.05 μM NaOH. The lower curve (-···-) reveals the differences between observed (•••) and calculated (—) intensities of the refined parameters form Rietveld analysis and X-ray powder diffraction pattern (*Fd* 3 *m*, site: 8a: 1/8, 1/8, 1/8 and 16-hedra: site 16d: ½, ½, ½, 12-hedra). **(B)** An SEM image is shown of μm sized single crystals (bar scale ≈1.0 μm) and the overall morphology of this crystal type and the Miller indexed faces are shown in (C).

By using computer simulations with multi-slice calculations, the Lipid A-diphosphate structure was obtained. The image multi-slice image simulations were carried out for the 100kV TEM Joel Microscope (T 3010) with imaging facilities for hollow-cone illuminations and using the Cowley algorithm [46, 47]. In addition, after successful indexing of the X-ray diffraction profiles and the selected area diffraction pattern (SAED), after the successful indexing of the powder-diffraction patterns and the selected-area diffraction patterns, a Pawley refinement was performed, taking the following parameters into consideration: cell parameters, peak-profile parameters, background and zero shifts. Following this refinement, a structure solution was imitated using a direct-space Monte Carlo-simulated annealing approach and a full-profile comparison was implemented. By employing a global optimization algorithm, trial structures were continuously generated by modifications in the specified degrees of freedom, i.e. three translations, three rotations and the dihedral angles.

It was possible to show that most of the Lipid A-diphosphate particles were orientated in the [001] direction with respect to the substrate for one of the five deformed tetrahedral subunits, i.e., the fivefold axis was parallel to the surface of the substrate [48]. Due to the presence of Lipid A-diphosphate and the surface tension, the only growth in the direction of the fivefold axis of decahedra was possible, resulting in long rods.

Since $n = n^*$ (n^* = particle/length^3) the orientational entropy and the electrostatic repulsion of the free energy expression for these charged rods favor antiparallel alignment of the rods [45], this will give rise to a cubic lattice-like interparticle structures as noticed in Figure 5**(C).** For $n >> n^*$ and 10 μM NaOH a hexagonal packing of parallel rods can be

anticipated as an appropriate description. If one considers the correlation of nearest-neighbor rods of Lipid A –diphosphate, then a parallel alignment of nearest neighbor rods is observed with a local ordering parameter S = 0.07 at n = 2.8 n^*. Individual rod-shaped particles are noticed in Figure 5B whereas in Figure 5A N-regions of Lipid A-diphosphate particles are observed, where the particles exhibit parallel orientations, which may correspond to Sm precursors. When n is significantly increased, the Lipid A-diphosphate clusters grow laterally, their contours become clearer, and more layering of the clusters appear. The particle packing fraction ϕ_P for the Sm phase was estimated to 0.28. The Sm layer period and in-layer separation were calculated to be 2.8 and 2.4 nm, respectively, for n = 5.5 n^*.

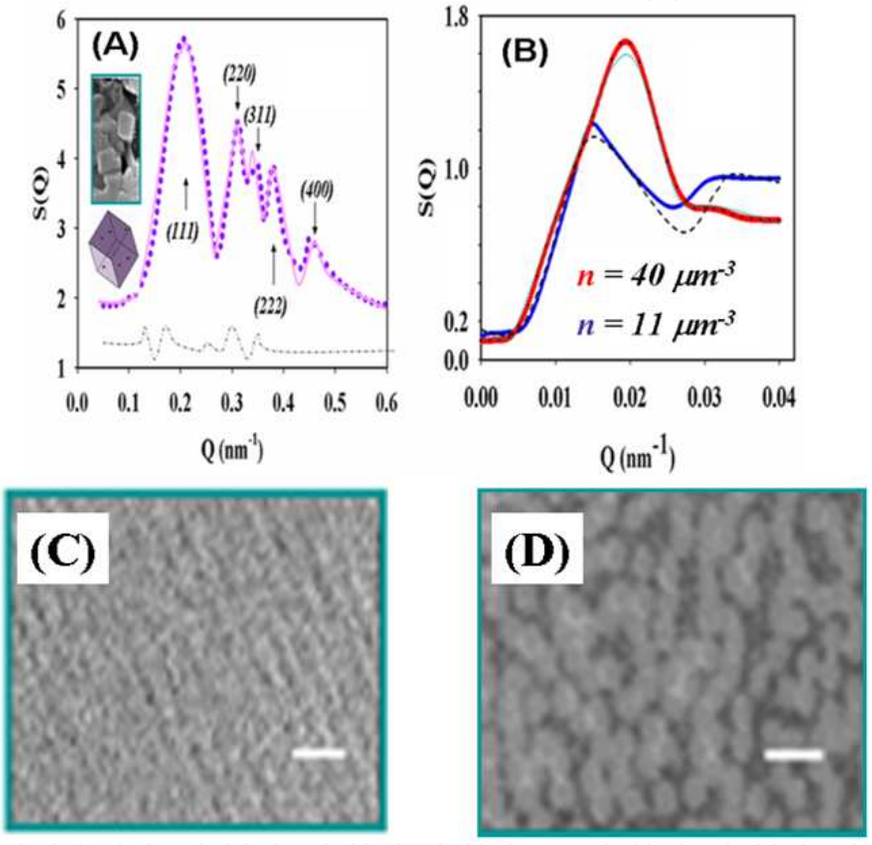

Figure 5. **(A)** S(Q) vs. Q profile for colloidal FCC-type crystals with a = 57.0 nm for n = 140 μm^{-3} and c_S = 2.05 μM NaOH. The lower curve (-·-·-) reveals the differences between observed (•••) and calculated (**—**) intensities of the refined parameters. The inset depicts a SEM image of single crystals (size ≈1.0 μm) and the morphology of this crystal type. **(B)** S(Q) vs. Q profiles as a function of n obtained by static light scattering for rods (**—**) and SAXS (**—**) at c_s = 7.6 μM NaOH, pH 7.85. These materials do not exhibit any iridescence. The dotted lines (**---**) represent the calculated S(Q) values for an isotropic solution of rods with L = 800 nm and d = 5.6 nm as a function of n; (·····) for a calculated dodecahedral Lipid A-diphosphate rod-model for n = 40 μm^{-3} (T = 295 K). **(C)** shows a high resolution electron micrograph (HTEM) image of highly ordered and crystalline Lipid A-diphosphate nanorods in the [100] direction observed at pH 7.85 approaching the melting line for n = 55 μm^{-3} (T = 295 K), the scale bar is 100 nm. **(D)** shows a HRTEM image of Lipid A-diphosphate observed at pH 7.85, crossing the melting line for n = 55 μm^{-3} (T = 295 K), and at 5 μM NaOH. The scale bar is also 100 nm.

3.3. Morphologies of Lipid A phosphates

The various morphologies of Lipid A-diphosphate and Lipid A-monophosphate nanocrystals as observed by SEM are shown in Figure 7.

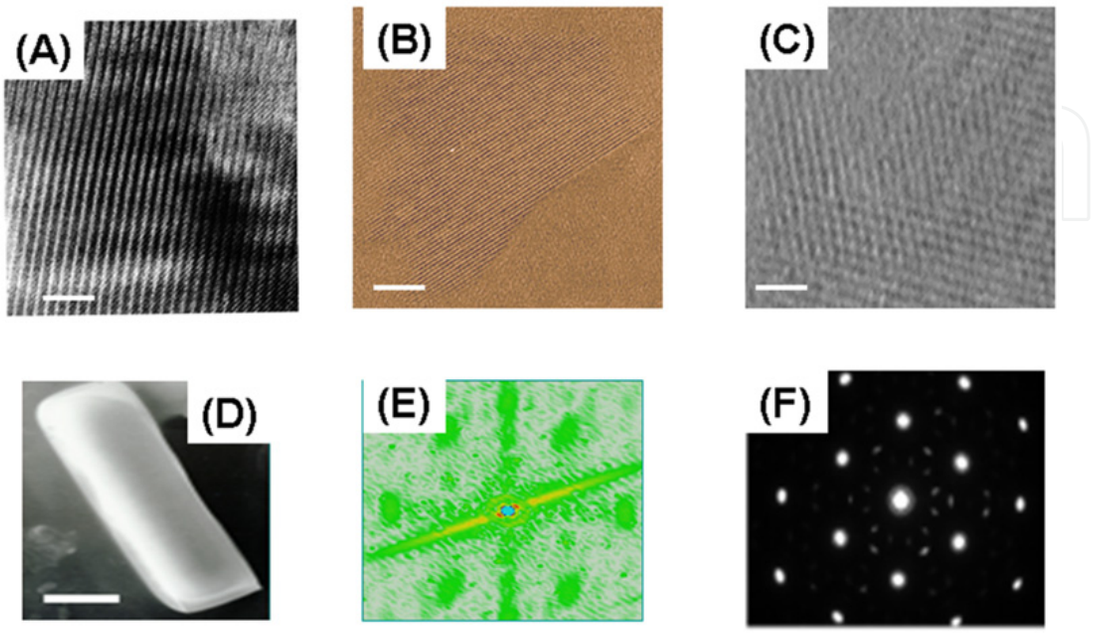

Figure 6. **(A) – (C)** show overviews of HRTEM images of crystalline Lipid A-diphosphate rods at pH 7.85 (295 K) along the [111] plane. The bar in (**A)** is 50 nm, 100 nm in **(B)** and 200 nm in **(C). (D)** Shows a long rod of Lipid A-diphosphate as a SEM image, the bar is 1 μm. This crystalline rod reveals FCC stacking faults along the [111] plane. A calculated Fourier transform image for models of truncated dodecahedral Lipid A-diphosphate particles is shown in **(E);** they are obtained form SAED pattern **(F)** from the lattices shown in **(A)** to (**C**). Model calculations support a five-fold axis in the [1-10] direction, and parallel to the (001) plane, i.e. 0° and 18°, but perpendicular to the fivefold axis **(E**) accounting for the experimental SAED pattern shown in **(F).**

These crystals are obtained at different particle number densities n as indicated and at constant T but at very low ionic strength, ($I \sim 10^{-6}$ M in NaCl or $I \sim 10^{-5}$ M in NaOH. Although the obtained nanocrystals at 10 μM NaOH show a better 3d order than those grown in very low NaCl concentrations according to the corresponding SAED and SAXS pattern quality, they generally reveal SEM images of icosahedral or dodecahedral morphology. Typical sizes of these crystals are of the order of 0.3-1 μm. Moreover, there was no congruent metastable other phases found for the icosahedral phase for the crystals grown in the presence of 10 μM NaOH, but there was in the presence of 1.0 μM NaCl, or 10 nM Ca^{2+} [11].]. Therefore, some small portion of FCC Lipid A-diphosphate was always present. Rhombic triacontahedral has been observed for Lipid A-monophosphate nanocrystals and is not the only icosahedral quasicrystal.

The antagonistic mediated incorporation into cubic crystalline Lipid A-diphosphate assemblies is more effective if the colloidal particles are oblate ellipsoids rather than curved. The assumed deformable soft spheres incorporate flexibility on a simple level [47]. At

mechanical equilibrium the soft Lipid A-diphosphate sphere may be approximated into a prolate or oblate ellipsoid of revolution while preserving its volume at $\pi d^3/6$ where d is the hydrodynamic diameter of the soft sphere (~ 7 nm). The distortion is given through the aspect ratio $\rho = a/b$ of the self-assembly, a is the symmetry semiaxis length of the ellipsoid and b is its orthogonal semiaxis length.

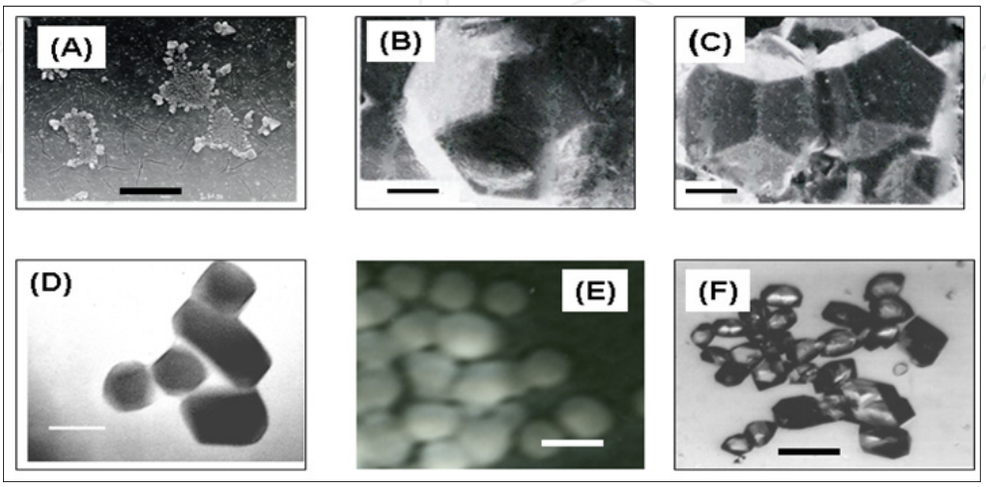

Figure 7. SEM images of the morphologies of Lipid A-diphosphate (**A** – **C**) and Lipid A-monophosphate crystals (**D** - **E**). These crystals are usually grown from aqueous dispersions containing either 10^{-5} M NaCl (A, B, E) or 10 μM NaOH (D, F). The icosahedral phase exhibits nanocrystals with pentagonal dodecahedral faceting. The scale bar is 100 nm in (A) - (C) and (E). The scale bar in (D) is 0.5 μm. In **(F**) faceted Lipid A-monophosphate nanocrystals are shown, the scale bar is 1.0 μm. The particle number density, n, was 350 μm^{-3} in (A) –(C), 150 μm^{-3} in (D) – (E), and 450 μm^{-3} in (F).

Furthermore, some Lipid A-diphosphate and approximants were formed by a peritectic reaction from the solid Lipid A-diphosphate phase and the liquid Lipid A-diphosphate (Form C of Fig. 1) at T = 295 K. These nanocrystals possess pentagonal dodecahedral solidification morphologies, but with exclusively pentagonal faces. Since this observation is associated with molecular motion and rearrangements of the positions in the Lipid A-phosphate nanocrystals lattices above a certain temperature (T > 295 K) or slowly cooling form T = 295 K to T = 288 K, which was deduced from broadening of the X-ray diffraction lines and SAED peaks, these modes belong to the phason long-wave-length phason. Relaxation of the phason strain is a diffusive process and therefore intimately related to the crystal growth process and is much slower than the phonon strain.

Quasicrystals exhibited non-crystallographic packing of non-identical Lipid A-phosphate spheres and a spatial packing of these spheres in either a cuboctahedron or an icosahedron were representative of sound physical models. Following an increase in temperature, a BCC phase was revealed and this structure gave rise to dodecagonal quasicrystals, which formed from spherical particles. Electron diffraction patterns of the dodecahedrons were recognized from the magnitudes of non-identical intensities of Lipid A-diphosphate and antagonistic Lipid A-diphosphate, which contained only 4 acyl-chains. It should be noted that the observed (3.3.4.3.4) was a crystalline analogue of

the above-mentioned icosahedral quasicrystal with a different length scale. The tiling pattern of triangles (N_3) and squares (N_4) where the vertices were surrounded by a triangle-square-triangle tiling pattern possessed a *p4gm* plane group. Another coded Lipid A-diphosphate approximant showed an 8/3 ratio with 6-fold symmetry and plane group *p6mm*. Both (3.3.4.3.4) and dodecagonal phases revealed a N_3/N_4 ratio of approx. 2.34; the ratio of the p6mm plane group was 8/3. Because bond orientational order existed, the direction of domains was classified into three orientations for the (3.3.4.3.4) tiling, but only two for the 8/3 approximants. The average magnitude of the prominent scattering vectors, $|Q| = 0.121$ nm^{-1}, and the length of sides of the triangles and of the squares was 50 nm.

3.4. Packing of Lipid A-phosphates

Under the assumption that the macroscopic shape of a crystal is related to its microscopic symmetry and taking the various X-ray diffraction patterns, the SAED's and the morphology into consideration, the Lipid A-diphosphate structures and their approximants can be reconciled by lowering the symmetry from cubic, $Im\bar{3}m$ or $Ia\bar{3}d$ (a = 4.55 nm) for the diphosphate or monophosphate, respectively, to rhombohedral $R\bar{3}m$, and finally to monoclinic ($P2_1$ or C2) which is acceptable if the Lipid A-phosphate anions were completely orientationally ordered [12]. This could be attributed to two different space-filling packings: (i) two dodecahedra on site **a** and six tetrakaidecahedra on site **d**, forming a $Pm\bar{3}n$ lattice; (ii) or sixteen dodecahedra on site **d** and eight hexadecahedra on site **a,** forming an $Fd\bar{3}m$ lattice (Fig. 8). The space-filling network of Lipid A-diphosphate consisting of slightly distorted polyhedra is reminiscent of the known basic frameworks of gas-hydrates and sodium silicon sodalites. The final geometry of the "spheres", i.e. whether they were rounded or faceted in shapes, was established. The equilibrium separation distance between the interfaces of the "spheres" suggested that they repel each other as a result of electrostatic, steric, van der Waals forces as well as water layer surrounding the spheres. The small cubic $Pm\bar{3}n$ (a = 6.35 nm) structure observed for the Lipid A-monophosphate clusters [38, 48], but different from the large cubic unit cell with a = 49.2 nm materialized as a result of a space-filling combination of two polyhedra, a dodecahedra and a tetrakaidodecahedra. This is in contrast to the tetrakaidecahedra ($Im\bar{3}m$) or rhombodo-decadecahedra ($Fd3m$) packings observed for the Lipid A-diphosphate assemblies (Fig. 8). The small cubic $Pm\bar{3}n$ (a = 6.35 nm) structure observed for the Lipid A-monophosphate clusters [38, 48], but different form the large cubic unit cell with a = 49.2 nm materialized as a result of a space-filling combination of two polyhedra, a dodecahedra and a tetrakaidodecahedra. This is in contrast to the tetrakaidecahedra ($Im\bar{3}m$) or rhombodo-decadecahedra ($Fd3m$) packings observed for the Lipid A-diphosphate assemblies. **Note:** The limited number of reflections observed for this large cubic unit cell in case of the Lipid A-monophosphate was not sufficient to discriminate between primitive and body-centered-cubic lattices, or more precisely between *Pn-n* and *I- - -* extinction groups. The two differ by the reflection condition *hkl: h=k+l=2n*, which satisfied the BCC lattice, but the first set of reflections on which this condition could

be tested would be the {421} reflection. This reflection was not observed because of the low resolution of the diffraction pattern.

Space groups such as $Im\bar{3}m$, $I4\bar{3}m$, $I4\bar{3}2$, etc. are all possible and may not be separated by extinction alone. Thus, it may be argued that favorable space filling packings will be achieved when satisfactory geometrical conditions were fulfilled (Plateaus's law). For the Lipid A-phosphates this resulted from minimizing the surface area between the aqueous films and so achieving a high homogeneous curvature. However, in the case of the Lipid A-monophosphate, rhombodo-decadecahedra ($Fd\bar{3}m$) packing seems to be suppressed a result of instability in the mean curvature between the tetrahedral and the octahedral nodes. Tetrakaidodecahedra packing shows only tetrahedral nodes. However, the tetrahedral angle (109.47°) can only be restored between all of the edges if the hexagonal faces of the truncated octahedron change and generate change and generate planer surfaces with no mean curvature and form Kelvin's minimal polyhedra [49,50].

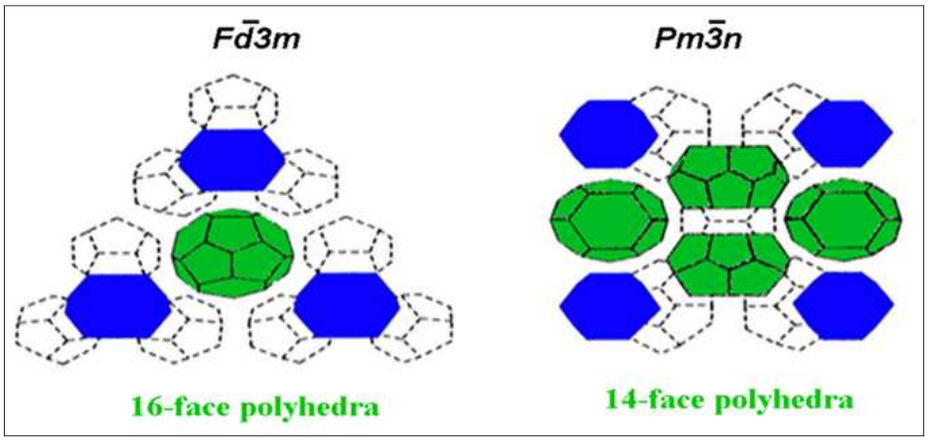

Figure 8. Packing of $Fd\bar{3}m$ and $Pm\bar{3}n$ tetrahedrally close-packed Lipid A-diphosphate and Lipid A-monophosphate structures for two cubic crystalline phases using Wigner-Seitz cells. For both structures, aqueous bilayer compartmentalizes the hydrophobic portion of the Lipid A-phosphates into tetrahedrally networks. This network is a combination of a pentagonal dodecahedron (blue) with 14 – face polyhedra (green) in $Pm\bar{3}n$ and with 16-face polyhedra (green) in $Fd\bar{3}m$.

4. Faceted crystal growth

4.1. Two-phase coexistence regions in monolayers

Normally equilibrium thermodynamics prevent faceting in two dimensions (2d) because the one-dimensional perimeter of a two-dimensional crystal exhibits no long-range order at any non-zero temperature. However, the formation of stable facets during crystallization need not prevent faceted crystal growth in two dimensions, which is supported both experimentally [18, 51-53] and by computer simulations [54-56]. This possibility is extremely useful in studies of cell surface recognition in the presence of Lipid A-diphosphate e.g. surface patterning, mechanical properties and cell mechanics with optical tweezers. Moreover, surface tension effects become important as the interface is no longer planar and

it introduces a length scale of the order of a few nm, influencing crystal shape, morphology and stability as well as biomineralization [57].

4.2. Surface-tension-gradient-induced crystal formation in monolayers

We observed a surface-tension gradient induced crystal growth phenomena in Lipid A-diphosphate and Lipid A-diphosphate approximants layers comprising of the same chemical composition as studied for the re-entrant phase BCC and FCC networks. Briefly, the surface tension gradient was created by heating the trough (1 cm^3, 5.0 mins/°C), measuring simultaneously the surface tension, γ, for various n, either in the presence of a fluorescent dye (Alexa Fluor 488, Molecular Probes USA) which was spread on the aqueous surface, or by direct observation with a Scanning Electron Microscope (SEM) when the samples were withdrawn from the container under a light microscope (Olympus BX 60) and transferred to a substrate, coated with Pt (1min) and studied in a SEM (JEOL 6400). A video recording system was hooked up to the light microscope for monitoring the morphology changes with time. Double-chained lipids reveal saturation coverage of ~1.0 molecule/0.5nm^2 in aqueous media, which are magnitudes different from Lipid A-diphosphate where ordering of Lipid A-diphosphate occurs at concentrations that are less than 1.33 x 10^{-11} mbar·s or saturation monolayer coverage of ~ 10^{-5} L [58, 59]. The surface density of the dye is ~ 10^{-2} molecule/nm^2. Since n is much lower than the CMC of Lipid A-diphosphate (14.0 μg/mL (3.5 x 10^{-5} mM) at 10°C and 7.5 μg/mL at 20°C (2.0 x 10^{-5} mM; Kraft point 5.8°C), the dye does not dissolve in the bulk phase, and because the measurements are far from the stability region of the Lipid A-diphosphate 3d crystals, the surface film is 2-dimensional. By compressing the monolayer film a liquid phase-liquid condensed phase coexistence space is reached. The coexistence phase is characteristic of the formation of dark and fractal like liquid condensed phase domain when viewed through the fluorescent microscope. The morphology of the various 2d Lipid A-diphosphate images and their evolution are depicted in Figure 9.

Faceted domains built up on the tip of the fractal branches, but these tips are not stable and after continuous crystal growth a dendritic pattern evolved. The domains are squeezed in-between the dendritic stems promote to grow. However, the external tips of the domains have a higher probability to expand into a dendritic pattern. It appears that the hexagonal shaped Lipid A-diphosphate crystals grew in the liquid-crystalline boundary (Fig. 9). It was also observed that the hexagonal domains enlarged to the dendritic pattern, where the corners of the hexagons are very sharp and the dendrites revealed stable tips and strong stems are clearly observed. Quantitatively, the Lipid A-diphosphate is higher than in the middle of the straight edge at the corners of the faceted pattern. This implies that the main transfer rate to the corners is higher than at other places in space causing an instability region. As a result the crystal edge corners grew more rapidly than the center region and (curled) dendrites appeared on the corners of the hexagon (Fig. 9g).

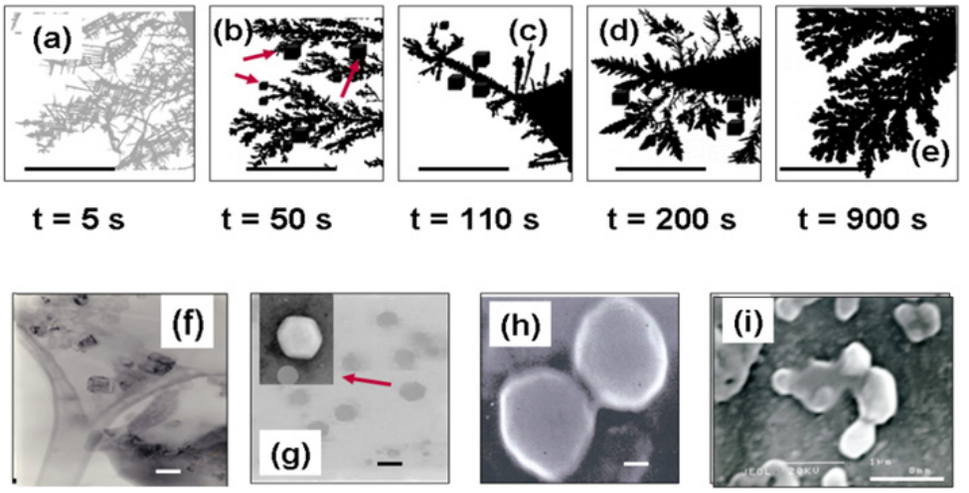

Figure 9. Development of fractal crystalline pattern of Lipid A-diphosphate domains as a function of time. The video-recorded light-optical microscopy images were directly converted to black and white images by using the Adobe Photoshop (version 8.0.1.) **(a)** Observed fractal patter when the monolayer of Lipid A-diphosphate is compressed to the liquid-crystalline to liquid-expanded coexistence region**. (b) – (e)** show the time evolution of the same Lipid A-diphosphate pattern from fractal to dendritic behavior under the microscope. At the tips (red arrows) in **(b & c)** become thicker and reveal facets; normally these tips grow into thick dendrites with clearly main stem, strong and stable tips **(d & e).** The bar size is 50 μm. The morphologies of the liquid-crystalline domains of Lipid A-diphosphate are shown **(f-i).** In **(f)** a HRTEM image of faceted cubic-like and unconnected Lipid A-diphosphate crystals are shown (the bar is 100 nm). **(g)** depicts the observed hexagon domain which grows usually near the cubic-like crystal domain; but this is dependent on T, however, at constant *I*; the bar size is 10 nm. **(h)** Shows a SEM image of fusing Lipid A-diphosphate crystals observed when the monolayer expands to a fluid state, or compresses to a certain density d_c where the crystals contact one another and fuse. The bar is 10 μm, T = 295 K and c = 6.0 μg/mL. **(i)** Shows single Lipid A-diphosphate nanocrystals grown at T = 295 k but in c = 60.0 μg/mL and in the presence of 20 μM NaOH. These nanocrystals exhibit icosahedral faces and also rhombic triacontahedral faceting; the bar size is 1 μm.

For this instability, a field gradient existed where crystals grew faster as they reached deeper into the gradient. As a result of this instability was an invasion of the more viscous phase by the less viscous phase without ordering or a characteristic length scale. It was also a process which operated during diffusion-limited aggreagtion, in which case the diffusive instability led to a fractal structure. Moreover, in the growth process far from equilibrium the aggregation of the fractal-like domains can be faster than the relaxation process of the Lipid A-diphosphate clusters. Hence the Lipid A-diphosphate clusters form rectangular lattices. The 2d-hexagonal domains nucleated and grew under lower force, where in the meantime the Lipid A-diphosphate clusters gain enough time to relax to minimum lattice energy positions. Therefore, the difference in macroscopic morphology together with the caused instability implies that, the structure of the liquid crystal domains depend on the driving force. Also what should be mentioned is the influence of different chiral conformers in the bulk solution whose presence has been supported by circular dichroism experiments and molecular simulations (unpublished results, 2011). The observed hexatic phase (Fig. 10), which separates the isotropic liquid Lipid A-

diphosphate cluster phase and the liquid crystalline phase has short-range translational and quasi long-range orientational order.

In accord with theory [22, 60-64] we are able to detect three phases: a liquid, hexatic and a crystal Lipid A-diphosphate phase, but no fluid-crystal or hexatic-crystal phase coexistence phase. This is supported from surface tensiometry measurements as a function of T and μg/mL bulk concentration revealing hexagonally shaped crystals.

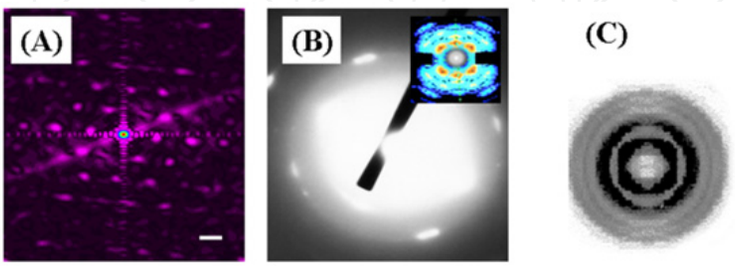

Figure 10. SAED's (Joel, T 3010, 300 kV, 15 cm) and SAXS images for the various crystalline Lipid A-diphosphate clusters at different μM NaOH and Lipid A-diphosphate concentrations (c). **(A)** SAED for a 2d-pattern, a 10 nm thick layer obtained from very small Lipid A-diphosphate crystallites (sizes ~ 0.1-0.2 μm, c = 3.5 μg/ml, T = 295 K and γ_c = 25.5 mN/m in 5 μM NaOH. This 2d pattern indicates a hexagonal or centered trigonal unit cell with a = 3.70 nm. The bar size is 0.5 nm^{-1}, and the image was obtained with a CCD camera. **(B)** Enlarged SAED pattern of a 2d crystallite for c = 8.5 μg/ml, T_c = 295 K and γ_c = 25.5 mN/m but for 5.75 μM NaOH. This crystalline Lipid A-diphosphate material is maintained for approximately 1-1.5 h., and is indicative for the hexatic phase (inset). **(C)** SAXS pattern for the fluid phase where only diffuse rings but no dots are visible and close to the melting line; a change from solid to liquid occurred ($d\gamma/dT < 0$, $S_s > S_b$) where S_s is larger than the bulk entropy (S_b) and where the density is very similar to that of the bulk (for $T > T_c$).

Normally, lipids or surfactant concentrations are well in the range of mM (mg/mL) when forming a liquid-like monolayer, but in the case of Lipid A-diphosphate we are in the μg/ml range or lower and strongly dependent on polydispersity in charge and size distribution! This is significantly different from insoluble surfactant monolayers. Preliminary theoretical fitting results of the thermodynamics, γ(T) vs. T ($T < T_c$), with T_c is the critical temperature where the slope changed $(d\gamma/dT)_c$, yielded values for the chain interactions of $b \cong 41.8\ k_BT$ and the effective sugar-phosphate headgroup attraction of $a \cong -6.6\ k_BT$ [58].

Different phase can be distinguished from 2d structure factors (Fig. 10). The functional form of the angular intensity profile of S(Q) is the square root Lorenzian of the hexatic phase and Lorenzian of the crystal phase [65, 66]. In the hexatic phase both the ring and the six spots (Fig. 10A & B) are clearly noticeable, where the six spots indicate a small ordered patchy like located in the dense liquid Lipid A-diphosphate dispersion (Fig. 10C). Using the disorder parameter ⟨D⟩ [67, 68], which is a function of T, the solid hexatic phase and the liquid phase reveal different slopes [69]. In the hexatic phase both ⟨D⟩ and the variance sharply increases with configurational temperature. Approaching the melting region close to the liquid phase the average and the variance of ⟨D⟩ approaches ~5.0 and 4.0, respectively, where $\langle D \rangle_j = 0$ corresponds to a perfect triangular lattice and becomes larger for more disordered structures. The thermal fluctuation and entropic interactions lower the free energy (Eq. 1) of

the interface when two Lipid A-diphosphate particles approach each other in a sort of Casimir type of effective attraction [70-72]. The polydispersity influences the coexistence region of the fluid and crystal to higher volume fractions. At fixed supersaturation, the height of the nucleation barrier is not affected by a polydispersity up to ~ 6% in our experimental studies; while for larger polydispersities the barrier increases sharply; thus an increase in surface tension γ with T and n is noticed.

But, when melting of Lipid A-diphosphate crystals commenced above a critical temperature (T_c), γ_c as a function of n, the evaporation rate becomes slower when the crystallites shrink. These crystallites may sediment rapidly when transforming into the bulk liquid with a higher density than from the onset of the crystallization, where a lower density of the bulk solution is met than the actual crystal and evaporates swiftly. This melting scenario is reminiscent to the coexistence of a dense and expanded crystal phase. This Lipid A-diphosphate crystal phase also depends strongly on polydispersity in size, mass and charge for T and n is constant. The total number of Lipid A-diphosphate crystals depends on the kinetics during the monolayer compression and is a function of n, T and γ. Once the early seed have developed the number of domains is fixed and does not change with subsequent compression unless the monolayer expands to a fluid state, or compresses to a certain density d_c where the crystals contact one another and fuse (Fig. 8h). Evidently this depends on the rate of compression (or evaporation) or "impurities" seen as "various Lipid A-diphosphate conformers" present in the bulk Lipid A-diphosphate dispersion due to the conformational changes of the disaccharide as noticed from the crystal structures of Lipid A-monophosphate [73]. The cause of this resulting instability originates from an increase of lipid A-phosphate conformers over another conformer on a characteristic length scale rather than on impurities [74]. It is also a process which operated during diffusion-limited aggreagtion, in which case the diffusive instability led to a fractal structure. Furthermore, the shape of the Lipid A-diphosphate crystals (Fig. 8A) is also affected by the interfacial free energy between the solid and liquid phase. Particularly, the interface influences the free energy penalty Aγ, which is proportional to the area of the interface and the surface energy γ. Consequently, the free energy difference of the crystal and the fluid is:

$$\Delta G = A \cdot \gamma - V \cdot n_{crystal} \Delta \mu \quad (1)$$

Where V is the volume of the crystal nucleus, $n_{crystal}$ is the particle number density in the crystal and $\Delta\mu = \mu_{Fluid} - \mu_{crystal}$ is the difference of the chemical potential of fluid and crystal, respectively.

Furthermore, the 2d order quality of the Lipid A-diphosphate crystals is influenced by grains due to mixed sizes and shapes (Fig. 9C). Complete uniformity cannot be expected. Assuming the 2d lattice and the force between adjacent spheres (or ellipsoidal particles with a low axial ratio) are identical may yield under compression (sedimentation, gravity, capillary forces) another packing than hexagonal resulting in change to a cubic lattice. This cubic lattice has actually been found for both lipids. Consequently the ordered 2d hexagonal structure which is present in the fluid state in the presence of μM NaOH (Fig. 2B) has a

minimum density, whereas the intermediate density rests with the detected cubic structure and finally the maximum density will be closer to the hexagonal close packing than to the simple cubic structure. This is contrary for the Lipid A-diphosphate invariant to the particle number density, n, and T=constant, but at very low I of μM to mM NaCl or nM Ca^{2+}, respectively [9, 11].

The influence of the Lipid A-diphosphate crystal-crystal-coexistence within the crystallization process has also to be considered. Since there is a noticeable variation in large and small μm-sized crystals as a function of polydispersity in size and charge, the ratio may be important so that the expanded Lipid A-diphosphate crystal phase is metastabile and a function of ϕ, T and I. As a result the density of the Lipid A-diphosphate nuclei is increasing with ϕ (n), which is contrary of the classical nucleation theory (CNT) [60]. According to this theory the density of the crystal is the same as the bulk density, or the density decreases with increasing of the Young-Laplace pressure, $\Pi_c = \gamma/L_c = \gamma \cdot g$, where L_c is the capillary length and depends on the curvatures inside and outside of the nuclei, due to capillary forces [74, 75], which takes also the surface tension and the chemical potential (μ) into account. Thus the assumption of CNT is independent on γ is no longer valid. This result in a decrease of the nucleation rate with an increase in supersaturation is governed by the increase in γ rather by slowing down the kinetics. There is also strong evidence that the 2 d crystals of Lipid A-diphosphate do not melt in a first-order transition but may be in second-order transition. This behavior follows the theory developed by Kosterlitz, Thouless, Halperin, Nelson, and Young (KTHNY), which predicts that a third phase, namely the hexatic phase with short-range translational order and quasi-long-range order exists between crystal and liquid [60-64].

5. Conclusion

The successful production of Lipid A-phosphate crystals makes it extremely useful to study various Lipid A-diphosphate assemblies of e.g. four, three, and penta- or hexaacylated Lipid A-phosphate approximants including those of modified disaccharide or monosaccharide moieties. This still remains to be elucidated. It was possible to construct different Wigner-Seitz polyhedra that make up the overall volume of the Frank-Kasper type unit cells with complexes comprised of Lipid A-diphosphate, antagonistic and non-toxic Lipid A-phosphate analogues depending on volume fraction, ϕ ($\phi = \upsilon_2 \cdot c$), the nature of the counterions and temperature. They form by spontaneous self-assembly and appear to obey the principles of thermodynamically reversible self-assembly but once self-assembled strongly resist disassembly. Base on these principles, Lipid A-phosphate assemblies can be designed which form large unit cells by containing more than hundreds of Lipid A-phosphates. The range of Lipid A-phosphate structures may also be increased further by employing various different ("non-identical subunits") and identical subunits of Lipid A-phosphate in analogy with block copolymers. The rational design of such assemblies and the nucleation and creation of polymorphic Lipid A-phosphates production of mesoscopic suitable cellular networks, and structure-function relationships will be impacted by a theoretical and practical understanding of the spherical assemblies, rod-like assemblies and

the mixtures thereof. Furthermore, the unit cell found for a four-single-chained Lipid A-phosphate approximant contained four honeycomb cells: two triangular and two quadrangular. However, the corresponding monophosphate contained 16 cells, of which either 10% or 66% were quadrangular. Given the theoretical and practical importance of this system, we expect that the attention given to it will substantially increase our knowledge on Lipid A-di-and monophosphates and the driving forces for the ordered assemblies. Furthermore, the structure of the Lipid A-diphosphate rod can be explained as truncated large dodecahedra.

The crystallization and phase behaviour of the Lipid A-diphosphate in two-dimensional (2d) and three-dimensional (3d) systems has been elucidated in more detail than before and analyzed as a function of ϕ, T, γ, morphology, and structure stability with the application of the CNT and KTHNY theories. But the experimental situation appear to be more complicated, because no real long-range translational order exists in 2d crystals and the phase behaviour close to freezing has been found to be richer than in 3d systems. We discovered for the Lipid A-diphosphate system a hexatic phase with short-range-translational order and quasi-long-range orientational order between crystal and liquid.

Author details

Henrich H. Paradies, Hendrik Reichelt and Chester A. Faunce
The University of Salford, Joule Physics Laboratory, Manchester, United Kingdom

Peter Quitschau
Fachhochschule Südwestfalen, University of Applied Sciences, Biotechnology & Physical Chemistry, Iserlohn, Germany

Kurt Zimmermann
The Symbio Herborn Group Inc., Institute for Microecology, Herborn, Germany

Acknowledgement

The authors thank Professors S. E. Donnelly, Drs. N. M. Boag, S. Simpson (Manchester, U.K.) for very critical discussions on electron microscopy, X-ray diffraction and chirality, and for using the High Resolution Electron Microscope (Joel T 3010) and the X-ray diffraction equipments. Professor K. Stadtlander (Iserlohn, Germany) for lending us the Olympus light microscope and the video camera. Financial support from the Biomaterials Project (Bruxelles, Grant BMH4-CT-96-0013), Chemical-Biotechnological Laboratories Inc (Iserlohn) and from Orthomol (Langenfeld, Germany) are gratefully acknowledged.

6. References

[1] Kepler, J. (1611). *De Nive Sexangula Godfrey Tampach*. Frankfurt am Main.
[2] Tiller, W. A. (1991). *The Science of Crystallization*. Cambridge University Press, Cambridge. (1991.

[3] Klug, A, Franklin, R. E., Humphreys-Owen, S. P. F. (1959). The Crystal Structure of Tipula Iridescent Virus As Determined By Bragg Reflection of Visible Light Biochim. *Biophys. Acta*, 32, 203-219.

[4] Holmes, K. C., Finch, J. T. (1967). Structural Studies of Viruses. *In Methods of Virology*, Vol. III, 351-474.

[5] Jones, R. A. L. (2002). *Soft Condensed Matter*. Oxford Master Series In Condensed Matter Physics, Oxfords University Press.

[6] Kittel, Ch. (1996). *Introduction to Solid State Physics*, John Wiley & Sons, Inc. New York.

[7] Thies, M., Quitschau, Zimmermann, K., Rusch, V., Faunce, A. C., Paradies, H. H (2002). Liquid-like ordered colloidal suspensions of Lipid A: The influence of Lipid A particle concentration, *J. Chem. Phys*. 116, 3471-3483.

[8] Faunce, C. A., Quitschau, P., Thies, M. Scheidt, T, Paradies, H. H. (2002). Bacteria and Bacterial fragments as Immunomodulatory Agents, in Probiotics, *Old Herborn University Seminar* Vol. 15, 95-120.

[9] Faunce, C. A., Quitschau, P., Paradies, H. H. (2003). Solution and structural properties of colloidal charged Lipid A (diphosphate) dispersions. *J. Phys. Chem. B.* 107, 2214-2227.

[10] Faunce, C. A., Paradies, H. H. (2007). Density fluctuation in Coulombic colloid dispersion: self-assembly of Lipid A-phosphates. *Mater. Res. Soc. Symp. Proc*. Vol. 947, 0947-A03-11.

[11] Faunce, C. A., Reichelt, H., Quitschau, P. Zimmermann, K., Paradies, H. H. (2005). The liquidlike ordering of Lipid A-diphosphate colloidal crystals: The influence of Ca^{2+}, Mg^{2+}, Na^{+}, and K^{+} on the ordering of colloidal suspensions of Lipid A-diphosphate in aqueous solutions. *J. Chem. Phys*. 122, 214727-214750.

[12] Faunce, C. A., Reichelt, H., Paradies, H. H., Quitschau, P. Rusch, V., Zimmermann, K. (2003). The formation of colloidal crystals of Lipid A-diphosphate: Evidence for the formation of nanocrystals at low ionic strength. *J. Phys. Chem. B*. 107, 9943-47.

[13] Paradies, H. H., Habben, F. (1993). Structure of N-hexadecylpyridinium chloride monohydrate. *Acta Crystallograph*. C 49, 744-747.

[14] Alonso, B., Massiot, D., Florian, P., Paradies, H. H., Gaveau, P., Mineva, T. (2009). ^{14}N and ^{81}Br. Quadrupolar nuclei as sensitive NMR probes of n-alkyltrimethylammonium bromide crystal structures. An experimental and theoretical study. *J. Phys. Chem. B*. 113, 11906-11920.

[15] Paradies, H. H., Clancy, S. F. (2000*).* Crystalline Polymorphism of Cetyltrimethyl-ammonium bromide and Distearyldimethyl ammonium (DSDMA) Compounds, *Rigaku J.* 17, 20.

[16] De Gennes, P., and Prost, J. (1993). *The Physics of Liquid Crystals*. International Series of Monographs on Physics. Oxford Science Publications (Clarendon Press, Oxford).

[17] Faunce, C. A., Paradies, H. H. (2009). Two new colloidal crystal phases of Lipid A-monophosphate: Order-to-order transition in colloidal crystals. J. Chem. Phys., 131, 244708-244728.

[18] Berge, B., Faucheux, L., Schwab, K., Libchaber, A. (1991). Faceted crystal growth in two dimensions, *Nature* 350, 322-324.

[19] Hamley (2000). *Introduction to Soft Matter* (2nd Edit.) J. Wiley, Chichester, U.K.

[20] Israelachvili, J. (1992). *Intermolecular and Surface Forces* (2nd Edit.), Academic Press.
[21] Hynninen, A.P., Thijssen, J. H. J., Vermolen, E. C. M. , Dijkstra, M., van Blaaderen, A. (2007). Self-assembly route for photonic crystals with a bandgap in the visible region. *Nat. Materials* 6, 202-205.
[22] Gasser, U. (2009). Crystallization in three-and two-dimensional colloidal suspensions. *J. Phys.: Condes. Matter* 21, 203101-2031025.
[23] Pieranski, P. (1980). Two-dimensional Interfacial Colloidal Crystals. *Phys. Rev. Lett* 45, 569-572.
[24] Sommerdijk, W. A., Cölfen, H. (2010). Lessons from Nature-Biomimetic Approaches to Mineral with Complex Structures. *MRS Bulletin*, 35 (2) 116-121.
[25] Garcia-Ruiz, J. M., Hyde, S. T., Carnerup, A. M., Christy, A.G., van Kranendonk, M. J., Welham, N. J. (2003). Self-assembled-carbonate Structures and detection of Ancient Microfossil. *Science* 302, 1194-1197.
[26] Crocker, J.C., Grier, D.G. (1998) From Dynamics to Devices: Directed Self-Assembly of Colloidal Material. *MRS Bulletin* Vol.23 (10) 24-50.
[27] Weitz, D. A., Russel, W.B. (2004). New Developments in Colloid Science. *MRS Bulletin* Vol. 9 (2) 82-105.
[28] Raetz, C. R., Whitefield, C. (2002). *Lipopolysaccharide endotoxins*. Ann. Rev. Biochem., 71, 635-700.
[29] Morbidity and Mortality Weekly Report; Technical Report No: 46 (1997); Center for Disease Control: Atlanta, GA, 941-944.
[30] Christ, W. J., Hawkins, L. D., Lewis, M. D., Kishi, Y. (2003*).* Synthetic Lipid A antagonist for sepsis treatment. In "*Carbohydrate-based Drug Discovery*", Vol. 1, pp 341-355; Ed. C.-H. Wong, Wiley-VCH Verlag GmbH & Co, KGA.
[31] Wehkamp, J., Bals, R., Kreft, B., Schroeder, J.-M., Stange, E. F. (2007). Innate Immunity. *Dtsch. Ärztebl, 104 (5),* A 257 – 262.
[32] Brandenburg, K., Koch M. H., Seydel, U. (1990). Phase diagram of Lipid A from Salmonella minnesota and Escherichia coli rough mutant lipopolysaccharide. *J. Struct. Boil.* 105, 11-21.
[33] Brandenburg, K., Richter, W., Koch M. H., Seydel, U (1998). The nonlamellar cubic and HII structures of Lipid A from Salmonella enterica serovar Minnesota by X-ray diffraction and freeze-fracture electron microscopy. *Chem. Phys. Lipids* 91, 53-69.
[34] Gast, E.P., Russel, W.B., Hall, C.K. (1986). An experimental and theoretical study of phase transitions in the polystyrene latex and hydroxyethylcellulose system. *J. Colloid Interface Sci* 109, 161-171.
[35] Reichelt, H., Faunce, C. A., Paradies, H. H. (2008). The phase transition of charged colloidal Lipid A-diphosphate. *J. Phys. Chem*. 112, 3290-3293.
[36] Robbins, M...O., Kremer, K., Grest, G.S. (1988). Phase diagram and dynamics of Yukawa systems. *J. Chem. Phys*. 88, 3286-3312.
[37] Meijer, E. J., Frenkel (1991). Melting line of Yukawa system by computer simulation. *J. Chem. Phys.* 94, 2269-2271.
[38] Faunce, C. A., Reichelt, H., Quitschau, P., Paradies, H. H. (2007). Ordering of Lipid A-monophosphate clusters in aqueous solutions. *J. Chem. Phys*. 127, 115103-11525.

[39] Lindemann, F. A. (1910). Über die Berechnung molekularer Eigenfrequenzen. *Phys. Z.* 14, 609-612.
[40] Strandburg, K.J. (1988). Two-dimensional melting. *Rev. Mood. Phys*. 60, 161-207.
[41] Löwen H., Palberg, T., Simon, R. (1993). Dynamic criterion for freezing of colloidal liquids. *Phys. Rev. Lett.* 70, 1557-1470.
[42] Verlet, L, Hansen, J.-P. (1969). Phase transitions of Lennard-Jones Systems. *Phys. Rev.* 184, 151-161.
[43] International Tables for X-ray Crystallography, Vol. 1, published for The International union of Crystallography, Birmingham, England 1965.
[44] Aschauer, H., Grob, A., Hildebrandt, J., Schuetze, E., Stuetz, P. (1990). Highly purified lipid X is an LPS-antagonist only. I. Isolation and characterization of immunostimulating contaminants in a batch of synthetic lipid X. *J. Biol. Chem*. 265, 9159-9164.
[45] Faunce, C. A., Paradies, H. H. (2008). Observations of liquid like order of charged rodlike Lipid A-diphosphate assemblies at pH 8.5. *J. Chem. Phys*. 128, 065105-065113.
[46] Cowley, J. M., Moodie, A. F., The scattering of electrons by atoms and crystals (1957). *Acta Crystallograph.* 10, 609-619.
[47] Goodman, P., Moodie, A. F., Numerical evaluation of N-beam wave functions in electron scattering by multi-slice method (1974). *Acta Crystallograph.* A30, 280-290.
[48] Paradies, H. H., Faunce, C. A., Thompson, R. (2005). Probing Complex Fluid Membranes and Films with Neutron Spin-Echo, Indiana University, August 14-17, (2005): http://www.iucf.indiana.edu/events/neutronmembrane/presentations/Paradies_lipid_diphosphates.pdf.
[49] Batista, V. M. O., Miller, M. A. (2010) Crystallisation of deformable spherical colloids. *Phys. Rev. Lett*. 105, 088305-088309.
[50] Faunce, C. A., Paradies, H. H. (2009). Two new colloidal crystal phases of Lipid A-monophosphate: Order-to-order transition in colloidal crystals. *J. Chem. Phys.* 244708-244728.
[51] Ziherl, P. and Kamien, R. D. (2001). Maximizing Entropy by Minimizing Area: Towards a New Principle of Self-Organization. *J. Phys. Chem. B* 105, 10147-10158.
[52] Anderson, D. M., Gruner, S. M., Leibler S. (1988). Geometrical aspects of the frustration in the cubic phases of lyotropic liquid crystals. *Proc. Natl. Acad. Sci.* USA, 85, 5364-5369.
[53] Miller, A. Knoll, Möhwald, H (1986). Fractal growth of Crystalline Phospholip Domains in Monomolecular Layers. *Phys. Rev. Lett* 56, 2633-36.
[54] Wang, M, Wildburg, G., van Esch, J.H., Bennema, P., Nolte, R.J.M., Ringsdorf (1993). Surface-tension-gradient-induced pattern Formation in Monolayers. *Phys. Rev. Lett*. 71, 4003-4006.
[55] McConnell, H.M., Keller, D, Gaub, H. (1986). Thermodynamic Models for the Shapes of Monolayer crystals. *J. Phys. Chem*. 90, 1717-1721.
[56] Meakin, P. (1988). Noise-reduced and anisotropy-enhanced Eden and screened-growth models. *Phys. Rev. A* 38, 418-426.

[57] Ben-Jacob, E., Garik, P. (1990). The formation of patterns in non-equilibrium growth. *Nature* 343, 523-530.

[58] Xiao, R.-F, Alexander, J.I.D., Rosenberger, F. (1988). Morphological evolution of growing crystals: A Monte Carlo simulation. *Phys. Rev. A* 38, 2447-2456.

[59] Faunce, C.A., Paradies, H.H. (2008). Nucleation of Calcium Carbonate as Polymorphic Crystals in the Presence of Lipid A-diphosphate. *J. Phys. Chem. B*., 112, 8859-8862.

[60] Faunce, C.A., Paradies, H.H. (2012). Observations of solution growth of nanocrystals of charged lipid A-diphosphate. *Phys. Chem. Lett.* Submitted.

[61] Lin, I.-H, Miller, D.S., Murphy, C.J., de Pablo, J. Abbott, N.L. (2011). Endotoxin-induced-Structural Transformations in Liquid Crystalline Liquids. *Science* 332, 1297-1300.

[62] Volmer, M., Weber, A., (1926). Germ formation in oversaturated figures. *Z. Phys. Chem.* 119, 277-301.

[63] Becker, R., Döring, W. (1935). Kinetic treatment of germ formation in supersaturated vapour. *Ann. Phys*. 24, 719-752.

[64] Young, A.P. (1979). Melting and the vector Coulomb gas in two dimensions. *Phys. Rev. B* 19, 1855-1866.

[65] Nelson, d. R., Halperin, B.I. (1979). Dislocation-mediated melting in two dimensions. *Phys. Rev. B*. 19, 2457-2484.

[66] von Grünberg, H.H., Keim, P., Maret, G. (2007). Phase transitions in Two-dimensional colloidal systems. *Soft Matter, Colloidal Order: Entropic and Surface Forces,* Vol. 3, eds. G. Gomper & M. Schick (Weinheim: Wiley-VCH) 40-83.

[67] Marcus, A.H., Rice, S.A. (1996). Observations of First-Order Liquid-to-Hexatic and Hexatic- to-Solid Phase Transitions in Confined Colloidal Suspensions. *Phys. Rev. Lett*. 77, 2577-2580.

[68] Davey, S.C., Budai, J., Goodby, J.W., Pindak, R., Moncton, D. E. (1984). X-ray study of the Hexatic-B-Smectic A Phase Transition in liquid Cyrstal Films. *Phys. Rev. Lett*. 53, 2129-2132.

[69] Qi, W.-K., Wang, Z.-R., Han, Y., Chen, Y. (2010). Melting in two-dimensional Yukawa systems: A Brownian dynamics simulation. J. *Chem. Phys*. 133, 234508-234520.

[70] Larson, a. E., Grier, D.G., (1996). Melting of Metastabile Crystallites in Charge-Stabilized Colloidal Suspensions. *Phys. Rev. Lett*. 76, 3862-3865.

[71] Shiba, H., Onuki, A., Araki, T. (2009). Structural and dynamical heterogeneities in two-dimensional melting. *Europhys. Lett*. 86, 66004-66010.

[72] Nikolaides, M.G., Bausch, A.R., Hsu, M.F., Dinsmore, A.D., Brenner, M.P., Gay, C., Weitz, D.A. (2002) Electric-field-induced capillary attraction between like-charged particles at liquid interfaces. *Nature* 420, 299-301.

[73] Goulian, M., Bruinsma, R., Pincus, P (1993). Long-range forces in heterogeneous fluid membranes. *Europhys. Lett*. 22, 145-150.

[74] Golestanian, R., Goulian, M., Kardar, M (1996). Fluctuation-induced interactions between rods on a membrane. *Phys. Rev. E*. 54, 6725-6734.

[75] Faunce, C.A., Paradies, H.H. (2011). Studies on Structures of Lipid A-monophosphate clusters. *J. Chem. Phys*. 134, 104902-149016.

[76] Mullins, W.W. (1984). Thermodynamic equilibrium of a crystalline sphere in a fluid. *J. Chem. Phys.* 81, 1436-1442.
[77] Cacciuto, A. Frenkel. D. (2005*)*. Stresses inside critical nuclei. *J. Phys. Chem. B* 109, 6587-6594.

IntechOpen